

Non-Hermitian generalizations of extended Su-Schrieffer-Heeger models

Yan He¹ and Chih-Chun Chien²

¹*College of Physics, Sichuan University, Chengdu, Sichuan 610064, China**

²*Department of physics, University of California, Merced, CA 95343, USA.†*

Non-Hermitian generalizations of the Su-Schrieffer-Heeger (SSH) models with higher periods of the hopping coefficients, called the SSH3 and SSH4 models, are analyzed. Although the one-dimensional Hermitian SSH3 model is topologically trivial, the non-Hermitian generalization leads to a topological system due to a point gap on the complex plane. The non-Hermitian SSH3 model is characterized by the winding number and exhibits the non-Hermitian skin effect. Moreover, the SSH3 model has localized states and zero-energy state not associated with the topology. Meanwhile, the SSH4 model resembles the SSH model, and its non-Hermitian generalization also exhibits the non-Hermitian skin effect. A careful analysis of the non-Hermitian SSH4 model with different boundary conditions shows the bulk-boundary correspondence is restored with the help of the generalized Brillouin zone or the real-space winding number. The physics of the non-Hermitian SSH3 and SSH4 models may be tested in cold-atom or other simulators.

I. INTRODUCTION

The Su-Schrieffer-Heeger (SSH) model [1] has been a paradigm of one-dimensional topological insulators [2, 3]. In the simplest version, the SSH model describes non-interacting quantum particles hopping in a one-dimensional (1D) lattice with alternating hopping coefficients. The bulk-boundary correspondence of the SSH model [2] shows that with periodic boundary condition, the winding number serves as a topological invariant differentiating the two topologically distinct regimes determined by the ratio of the two hopping coefficients. With open boundary condition, localized edge states can be found at the ends of the system. Importantly, the number of edge states can be determined by the winding number. Originally proposed for polyacetylene [1], the SSH model has been demonstrated experimentally by cold-atoms in optical superlattices [4] and by chlorine atoms on copper surface [5] and many other quantum systems. Classical mechanical systems may also mimic the SSH model [6, 7].

There have been many generalizations of the SSH model. By considering the SSH model as a system with a periodic pattern of the hopping coefficients, there are two sites per unit cell due to the alternating hopping coefficients, so the period is two. One line of generalizations considers the effects of increasing the period of the patterns of hopping, and the models are usually known as the extended SSH models. Here we call the extended SSH models with period-3 and period-4 hopping coefficients the SSH3 and SSH4 models, respectively. Interestingly, the Hermitian SSH3 model is not topological because it lacks the chiral (sublattice) symmetry. While the SSH model belongs to the AIII class, the SSH3 model belongs to the A class and is topologically trivial in 1D [3, 8]. In contrast, the SSH4 model [9] is a topological insulator, and it is basically the SSH model in disguise. The SSH4

model has the chiral symmetry and belongs to the same class of the SSH model, and the winding number can characterize its band topology. The SSH4 model has four bands with more mid-gap states located inside the three gaps. However, only the zero-energy states are protected by the chiral symmetry while the other mid-gap states are not associated with the topology. In addition, the SSH4 model has a much larger parameter space and can display richer phenomena. While the SSH4 model has been demonstrated in cold-atom experiments [10], similar experiments are expected to realize the SSH3 model as well [8].

On the other hand, the SSH model has a Hermitian Hamiltonian. The formulation of non-Hermitian quantum mechanics [11–13] has introduced another line of generalizations of the SSH model. The non-Hermitian SSH model has been intensely studied [14–19] and, just like the paradigmatic Hermitian SSH model, become an important platform for investigating non-Hermitian topological phenomena. The results from the systems with periodic and open boundary conditions may no longer agree, and the introduction of the biorthonormal basis and generalized Brillouin zone are crucial in restoring the bulk-boundary correspondence in the non-Hermitian SSH model [14, 15, 18–21]. Moreover, the presence of asymmetric hopping coefficients between the same pair of sites leads to the non-Hermitian skin effect, where the bulk states exhibit skewed profiles [14, 22]. The classifications of non-Hermitian topological systems are also different from those of Hermitian topological systems [23–28].

Here we integrate the two lines of generalizations of the SSH model and investigate non-Hermitian SSH3 and SSH4 models. While the Hermitian SSH3 model is topologically trivial, a generalization to the non-Hermitian model leads to topological properties as the eigenstates encircle the origin on the complex plane, illustrating how non-Hermitian generalizations can change the physics of the Hermitian counterpart. Moreover, we will show two types of localized states not associated with the topology as well as a zero-energy state from a symmetry of

* heyancp@scu.edu.cn

† cchien5@ucmerced.edu

the non-Hermitian SSH3 model. On the other hand, the SSH4 model is already topological in the Hermitian case. Nevertheless, a non-Hermitian generalization of the SSH4 model shows the non-Hermitian skin effect, causing the skewed profiles of the bulk states. In addition, the energy spectrum and topological invariant of the non-Hermitian SSH4 model become sensitive to the boundary conditions, showing the typical behavior of non-Hermitian systems [14, 15]. There has been previous work on a non-Hermitian generalization of the SSH3 model [29], but the system has diagonal non-Hermitian terms rather than the off-diagonal non-Hermitian terms of the systems discussed here, leading to different physics.

The non-Hermitian SSH3 model will be shown to have a point gap, as all of its eigenvalues on the complex plane encircle a given point. Non-Hermitian models with point gaps have been studied in Ref. [30]. An important feature of the models with point gaps is that the 10-fold way classification of the Hermitian models collapses into a 6-fold way classification of the non-Hermitian models. Therefore, the symmetry classes of A, DIII and CI merge together into one. Because of the change of the classification, one can find a \mathcal{Z} topological index for the class A in 1D if the non-Hermitian model has a point gap. In such a case, the full spectrum is usually very sensitive to the boundary condition, giving rise to certain exotic bulk-boundary correspondence without a Hermitian counterpart. On the other hand, the non-Hermitian SSH4 model will be shown to have a line gap because its eigenvalues form several clusters that can be separated by lines on the complex plane. For models with line gaps, the usual 10-fold way classification of the Hermitian models is refined to a much more complicated classification [31]. As for the SSH4 model, the non-Hermitian generalization studied here resembles the Hermitian one. Nevertheless, the non-Hermitian skin effects will lead to quantitatively different results with different boundary conditions, so additional analyses are performed to restore the bulk-boundary correspondence of the non-Hermitian SSH4 model.

The rest of the paper is organized as follows. Section II summarizes the Hermitian SSH3 model and then presents its non-Hermitian generalization. We discuss the topological properties characterized by the energy

spectrum and winding number and analyze two localized edge states and a zero-energy state not associated with the topology. Section III reviews the Hermitian SSH4 model and then presents its non-Hermitian generalization. The results from the system with different boundary conditions differ from each other due to the non-Hermitian skin effect. We use the generalized Brillouin zone and real-space winding number to show that the bulk-boundary correspondence works for the non-Hermitian SSH4 model. Possible realizations of the non-Hermitian SSH3 and SSH4 models in ultracold atoms or other types of simulators are discussed in Section. IV. Finally, Section V concludes our work.

II. SSH3 MODEL

A. Hermitian model

We consider the Hermitian model with period-3 hopping coefficients, or the SSH3 model. This can be thought of as a generalization of the SSH model with three lattice sites in one unit cell. The real-space Hamiltonian is

$$H = \sum_j \left[t_1 c_{j,1}^\dagger c_{j,2} + t_2 c_{j,2}^\dagger c_{j,3} + t_3 c_{j,3}^\dagger c_{j+1,1} + h.c. \right] \quad (1)$$

Here the hopping coefficients $t_{1,2,3}$ are assumed to be real. In momentum space, the Bloch Hamiltonian is a 3 by 3 matrix:

$$H = \begin{pmatrix} 0 & t_1 & t_3 e^{-ik_x} \\ t_1 & 0 & t_2 \\ t_3 e^{ik_x} & t_3 & 0 \end{pmatrix}. \quad (2)$$

Here k_x is the crystal momentum. This model does not have parity, time-reversal, or chiral symmetry, and it belongs to the class A [3]. In 1D, the Hermitian models in class A are topological trivial.

The topological triviality of the Hermitian SSH3 model has been discussed in Ref. [8]. However, an extension of Eq. (2) to a 2D model can result in nonzero Chern numbers by introducing a fictitious periodic momentum k_y to modulate the hopping coefficients [8]. The Hamiltonian of the 2D model is given by

$$H_{2D} = \begin{pmatrix} 0 & t_1 \cos(k_y + \phi_1) & t_3 \cos(k_y + \phi_3) e^{-ik_x} \\ t_1 \cos(k_y + \phi_1) & 0 & t_2 \cos(k_y + \phi_2) \\ t_3 \cos(k_y + \phi_3) e^{ik_x} & t_2 \cos(k_y + \phi_2) & 0 \end{pmatrix}. \quad (3)$$

Here ϕ_i for $i = 1, 2, 3$ are some constant angles. One has to choose suitable values of $t_{1,2,3}$ to keep the gaps open. The Chern numbers of the three bands are $Ch = (2, -4, 2)$ for the generalized 2D Hermitian model [8].

B. Non-Hermitian generalization

Next, we introduce a non-Hermitian generalization of the SSH3 model. With periodic boundary condition, the

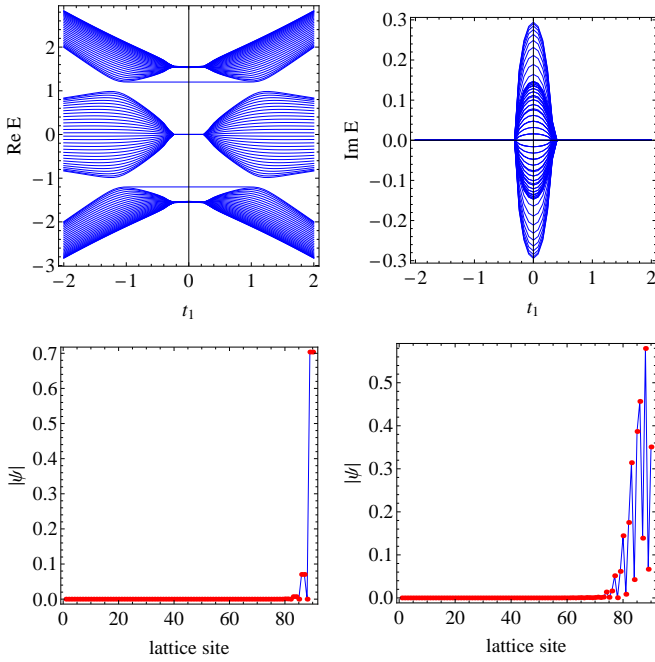


Figure 2. (Top row) The energy spectrum $\text{Re}E$ (left) and $\text{Im}E$ (right) of the non-Hermitian SSH3 model (8) with open boundary condition as a function of t_1 . Here $t_2 = 1.2$, $t_3 = 1$ and $\gamma = 0.3$. (Bottom row) The modulus of the wavefunctions of an edge state (left) and a bulk state (right), respectively. Here $t_1 = 0.5$, $t_2 = 1.2$, $t_3 = 1$, $\gamma = 0.3$, and $N = 90$.

gies, we use $H\psi = t_2\psi$ with $\psi = (a_1, \dots, a_N)^T$ to obtain

$$(t_1 - \gamma)a_{3n-2} - t_2a_{3n-1} + t_2a_{3n} = 0, \quad (9)$$

$$t_2a_{3n-1} - t_2a_{3n} + t_3a_{3n+1} = 0, \quad (10)$$

$$t_3a_{3n} - t_2a_{3n+1} + (t_1 + \gamma)a_{3n+2} = 0. \quad (11)$$

The boundary condition is given by $(t_1 + \gamma)a_2 - t_2a_1 = 0$ and $t_2a_{N-1} - t_2a_N = 0$. By assuming $a_N = 1$, we find

$$a_{3n-1} = a_{3n} = \left(\frac{t_1 + \gamma}{t_3}\right)^{M-n}, \quad a_{3n-2} = 0. \quad (12)$$

Here $n = 1, \dots, M$ and $M = N/3$. If we further assume that $t_1 + \gamma < t_3$, then the values of $a_{3n-1} = a_{3n}$ decay exponentially as n decreases. Therefore, the boundary condition $a_2 = 0$ is approximately satisfied. We thus found that the wavefunction (12) is an approximation of the mid-gap state with $E = t_2$. Similar results can be obtained for the state with $E = -t_2$. Therefore, the mid-gap states have a zero-amplitude point for every three sites. In contrast, the bulk states do not have such repeated zero-amplitude points. Checking the zero-amplitude points will help differentiate the mid-gap states from the bulk-states of the non-Hermitian SSH3 model in the presence of the non-Hermitian skin effect.

We want to point out those mid-gap edge states have nothing to do with the winding number shown in Eq. (7), and they are fragile against disorder. If a random hopping term is added to the SSH3 model, the mid-gap states

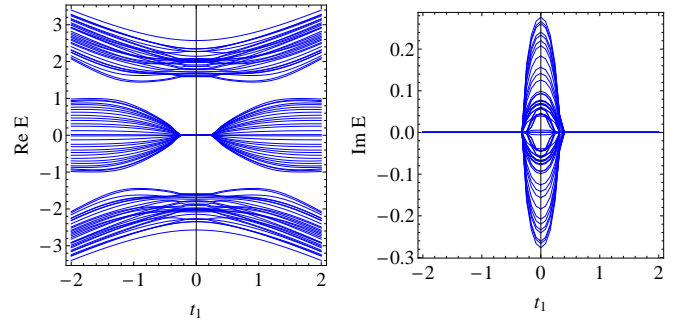


Figure 3. The real part (left panel) and imaginary part (right panel) of the energy spectrum of the non-Hermitian SSH3 model (13) with disorder and open boundary condition as a function of t_1 . In the presence of disorder, the mid-gap states merge into the bulk bands and are no longer visible. Here $t_2 = 1.2$, $t_3 = 1$ and $\gamma = 0.3$.

will merge into the bulk bands while the energy gaps remain open. To illustrate this feature, we introduce the following model

$$H_r = \sum_j \left[(t_1 + \gamma)c_{j,1}^\dagger c_{j,2} + (t_1 - \gamma)c_{j,2}^\dagger c_{j,1} \right] + \sum_j \left[t_2(1 + r_j)c_{j,2}^\dagger c_{j,3} + t_3c_{j,3}^\dagger c_{j+1,1} + h.c. \right]. \quad (13)$$

Here r_j are independent random variables uniformly distributed between 0 and 1. In Figure 3, we plot the energy spectrum of H_r . One can clearly see that the mid-gap states originally located at $E = \pm t_2$ merge into the bulk bands while the bandgaps remain open in the presence of disorder.

2. Non-topological edge states of type II

There are another type of localized states in the non-Hermitian SSH3 model. For the real-space Hamiltonian shown in Eq. (8) with $N = 3m + 2$ sites, there are two special states with the eigenvalues $E_{1,2} = \pm\sqrt{t_1^2 - \gamma^2}$ and the corresponding eigenvectors

$$\psi = (x_1, \dots, x_N)^T, \quad (14)$$

$$x_{3i+1} = r^i \left(-\frac{t_2}{t_3}\right)^i, \quad x_{3i+2} = \pm r^{i+1} \left(-\frac{t_2}{t_3}\right)^i,$$

for $i = 0, \dots, m$; $x_{3i+3} = 0$, for $i = 0, \dots, m-1$.

Here $r = \left(\frac{t_1 - \gamma}{t_1 + \gamma}\right)^{1/2}$. If $t_2 < t_3$ and $\gamma > 0$, the two states are localized at one end of the system. However, there is no such states for the $N = 3m$ and $N = 3m + 1$ cases. Therefore, the two localized states depend on the geometry, not the topology of the system.

The two localized states in the $N = 3m + 2$ case can be understood as follows. The Hamiltonian (8) with $N =$

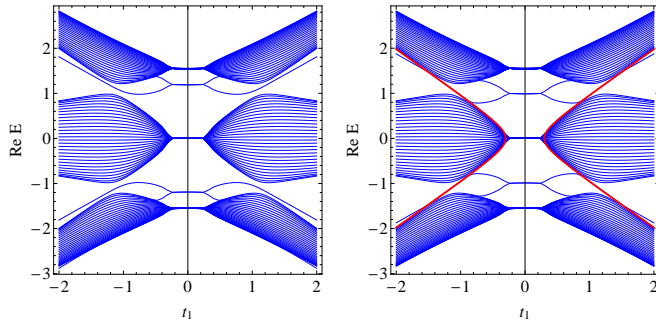


Figure 4. The energy spectrum ReE of the non-Hermitian SSH3 model (8) as a function of t_1 with $N = 92$ sites. The left and right panels show the case with $t_2 = 1.2$, $t_3 = 1$, and $\gamma = 0.3$ and the case with $t_2 = 1$, $t_3 = 1.2$, and $\gamma = 0.3$, respectively. The non-topological edge states (the thick red lines) only show up in the right panel.

$3m + 2$ can be rewritten as

$$H = H_1 + H_2, \quad (15)$$

$$H_1 = \text{diag}\{0, A, A, \dots, A, 0\}, \quad (15)$$

$$H_2 = \text{diag}\{B, 0, B, 0, \dots, 0, B\}, \quad (16)$$

$$A = \begin{pmatrix} 0 & t_2 & 0 \\ t_2 & 0 & t_3 \\ 0 & t_3 & 0 \end{pmatrix}, \quad B = \begin{pmatrix} 0 & t_1 + \gamma \\ t_1 - \gamma & 0 \end{pmatrix}. \quad (17)$$

Here 0 is a 1 by 1 matrix. The matrix A has a zero mode $\psi_0 = (1, 0, -t_2/t_3)^T$ satisfying $A\psi_0 = 0$. Therefore, H_1 also has a zero mode $\psi = (c_0, c_1\psi_0, c_2\psi_0, \dots, c_m\psi_0, c_{m+1})^T$. Next, one can check that the matrix B has the following eigenvectors

$$Bu_{1,2} = \pm \sqrt{t_1^2 - \gamma^2} u_{1,2}, \quad u_{1,2} = (1, \pm r)^T. \quad (18)$$

By operating H_2 on ψ , one can adjust the coefficients c_i to make ψ an eigenvector of H_2 . This procedure leads to the following conditions

$$c_{i+1}(\psi_0)_1 = \pm r c_i(\psi_0)_3, \quad i = 1, \dots, m-1; \quad (19)$$

$$c_1(\psi_0)_1 = \pm r c_0, \quad (20)$$

$$c_{m+1} = \pm r c_m(\psi_0)_3. \quad (21)$$

Hence, $c_{i+1}/c_i = \mp r(t_2/t_3)$. After setting $c_0 = 1$, we arrive at the two localized states shown in Eq. (14).

Here we emphasize that the localized states that we just presented are different from the mid-gap states discussed previously, despite the similarity between their wavefunction patterns. We will call the previous mid-gap states the type-I localized states and the localized states presented latter the type-II localized states. The type-II localized state requires two conditions: $t_2 < t_3$ and $N = 3m + 2$. In contrast, the type-I localized states are more general and do not require special lattice number or hopping coefficients. To illustrate the independence of the type-I and type-II localized states, we show in Figure

4 the energy spectrum of the non-Hermitian SSH3 model as a function of t_1 for the case with $N = 3m + 2$ sites. We compare a case with $t_2 > t_3$ in the left panel and a case with $t_2 < t_3$ in the right panel. The type-I localized states, corresponding to the short horizontal lines, are visible in both panels. In contrast, the type-II localized states, shown by the red diagonal lines, only exist in the right panel.

3. Zero-energy state

We mention there is a zero-energy state of the SSH3 model when $N = 2m + 1$ and $N \geq 5$. The zero-energy state is due to a symmetry of a tri-diagonal matrix with vanishing diagonal elements. The matrix $V = \text{diag}\{1, -1, 1, -1, \dots, -1, 1\}$ satisfies $VHV = -H$. If ψ is an eigenvector of H with the eigenvalue E , then $V\psi$ is an eigenvector of H with the eigenvalue $-E$. When the dimension of H is odd, there must be a zero-energy state. In the context of fermions in odd-number lattices, the zero-energy state has been discussed in Ref. [34] for Hermitian models. For the non-Hermitian model discussed here, the zero-energy state shows localization at one end. However, the localization of the zero-energy state is due to the non-Hermitian skin effect, not due to the topological property of the system. The zero-energy state may contribute a peak to the local density of state [8].

III. SSH4 MODEL

A. Hermitian model

After considering the SSH3 generalizations, we move on to the Hermitian model with four lattice-sites in one unit cell, known as the SSH4 model [9]. With periodic boundary condition, the Bloch Hamiltonian in momentum space is

$$H = \begin{pmatrix} 0 & t_1 & 0 & t_4 e^{-ik} \\ t_1 & 0 & t_2 & 0 \\ 0 & t_2 & 0 & t_3 \\ t_4 e^{ik} & 0 & t_3 & 0 \end{pmatrix}. \quad (22)$$

The eigenvalues are given by

$$E = \pm \left(\frac{B \pm \sqrt{B^2 - 4C}}{2} \right)^{1/2}, \quad B = t_1^2 + t_2^2 + t_3^2 + t_4^2, \quad (23)$$

$$C = (t_1 t_3)^2 + (t_2 t_4)^2 - 2t_1 t_2 t_3 t_4 \cos k.$$

There are four bands. If $t_1 t_3 = \pm t_2 t_4$, the gap between the middle two bands is closed at $k = 0$ or $k = \pi$.

We briefly summarize the symmetry of the SSH4 model. By introducing the matrix $\Gamma = I_2 \otimes \sigma_z$ with I_2 being the 2 by 2 identity matrix, one can verify that

$$\Gamma H + H \Gamma = 0. \quad (24)$$

and its solution is $|\beta| = \sqrt{\frac{t_1 - \gamma}{t_1 + \gamma}}$. Therefore, C_β is still a circle on the complex plane but with a radius smaller than 1.

To calculate the winding number, we again transform $H(\beta)$ to an off-diagonal form

$$SH(\beta)S^{-1} = \begin{pmatrix} 0 & g_1 \\ g_2 & 0 \end{pmatrix}, \quad (46)$$

$$g_1 = \begin{pmatrix} t_1 + \gamma & t_4\beta^{-1} \\ t_2 & t_3 \end{pmatrix}, \quad g_2 = \begin{pmatrix} t_1 - \gamma & t_2 \\ t_4\beta & t_3 \end{pmatrix}.$$

With the introduction of β , the winding number can be generalized to

$$W = \frac{1}{2\pi i} \int_0^{2\pi} d\theta z^{-1} \frac{dz}{d\theta}. \quad (47)$$

Here $z = \det(g_1) = (t_1 + \gamma)t_3 - t_2t_4|\beta|^{-1}e^{-i\theta}$. Then it can be shown that

$$W = \begin{cases} 1, & t_1 < \sqrt{\frac{(t_2t_4}{t_3})^2 + \gamma^2}; \\ 0, & t_1 > \sqrt{\frac{(t_2t_4}{t_3})^2 + \gamma^2}. \end{cases} \quad (48)$$

Therefore, the regime of nonzero winding number agrees with the appearance of the edge states computed from the case with open boundary condition.

In the second method, we directly calculate the winding number in real space with open boundary condition, following Refs. [35]. To achieve the goal, we need to obtain the left- and right- eigenvectors of Eq. (32), given by

$$H|u_n^R\rangle = E_n|u_n^R\rangle, \quad H^\dagger|u_n^L\rangle = E_n^*|u_n^L\rangle. \quad (49)$$

Those eigenvectors allow us to introduce the following Q -matrix:

$$Q = \sum_{\text{Re}E_n > 0} |u_n^R\rangle\langle u_n^L| - \sum_{\text{Re}E_n < 0} |u_n^R\rangle\langle u_n^L|, \quad (50)$$

satisfying $Q^2 = I$, where I is the identity operator. The real-space winding number [35–37] is then given by

$$W = \frac{1}{2L} \text{Tr}'(\Gamma_N Q[Q, X]). \quad (51)$$

Here $\Gamma_N = I_N \otimes \Gamma$ with I_N being the N by N identity matrix. We also define $X = X_1 \otimes I_4$ with the position operator $(X_1)_{ij} = i\delta_{ij}$. To eliminate the boundary effects, we divide the 1D system into three segments with lengths l , L , and l , satisfying $L + 2l = N$. The partial trace Tr' means the summation is only over the middle segment L . The real-space winding number W was first proposed by Kitaev [36] for a Hermitian 1D model with chiral symmetry. It has been shown to be the same as the momentum-space W if the grid size is large enough [36]. One should assume a large enough l in order to avoid the boundary effect, but there is no other constraint such as $l \ll L$. If calculated correctly, W should be real and quantized. However, the eigenvectors of the non-Hermitian model

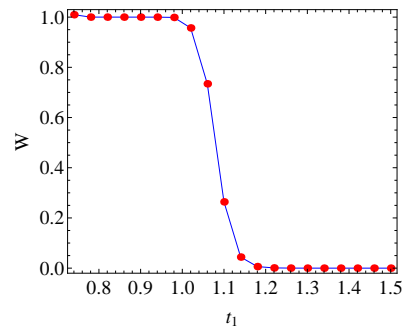


Figure 6. The real-space winding number, shown in Eq. (51), of the non-Hermitian SSH4 model as a function of t_1 . Here $t_2 = t_3 = t_4 = 1$ and $\gamma = 0.5$.

are calculated numerically and may be subjected to numerical errors, which in turn may cause a slight deviation of W from its quantized values.

Figure 6 shows the real-space winding number of Eq. (51) as a function of t_1 with $t_2 = t_3 = t_4 = 1$ and $\gamma = 0.5$. The grid size is $N = 50$ and we use $l = 10$. There is a transition of the values of W around $t_1 \approx 1.1$, which agrees with the location where the edge state emerges. Therefore, the bulk-boundary correspondence is restored for the non-Hermitian SSH4 model if the real-space W is considered.

IV. EXPERIMENTAL IMPLICATIONS

For the non-Hermitian SSH4 model, the winding number may be inferred from the so-called Zak phase [38], which is a measurable quantity used to identify the topology of the Hermitian SSH model [4] in cold atoms. The Zak phase can be obtained from a line integral of the Berry connection. Since the non-Hermitian SSH4 model has the bi-orthogonal eigenstates defined in Eq. (49), we introduce the non-Abelian Berry connections as

$$A_{mn}(k) = -i \sum_{m,n=1}^2 \langle u_m^L | \frac{\partial}{\partial k} | u_n^R \rangle. \quad (52)$$

Here we assume $E_1 < 0$ and $E_2 < 0$, referring to the two lowest energy states for a half-filled system, and the Berry connection defined above is a 2 by 2 matrix. In terms of this Berry connection, the Zak phase after the system traverses the Brillouin zone is introduced as

$$\theta = \oint dk \text{Tr} A(k). \quad (53)$$

Similar to the Hermitian case, there is a simple relation between the Zak phase and the winding number, given by $\theta = \pi W \pmod{2\pi}$. Explicitly, $\theta = 0$ if the winding number is even and $\theta = \pi$ if the winding number is odd. The Berry connection may also be thought of as the expectation value of the position operator because $\text{Tr} A = \sum_{n=1}^2 \langle u_n^L | x | u_n^R \rangle$. Therefore, the Zak phase

defined above also reflect the total polarization of the system with the lower two bands filled if the system is charged. On the other hand, the non-Hermitian SSH3 model lacks a topological Hermitian counterpart and the Zak phase cannot be directly applied.

The SSH model has been realized in experiments using ultracold atoms in optical potentials forming a 1D superlattice [4]. The Zak phase has been detected, showing a quantized difference between different topological regimes. The Hermitian SSH4 model has also been realized in cold-atom experiments [25]. The Hermitian SSH3 model has been proposed to be realizable using cold-atoms [8] as well. By coupling additional atoms in augmented optical potentials, non-Hermitian effects may be introduced to cold-atoms systems via the reservoir effects [39]. Given the rapid developments of trapping and manipulating cold-atoms, the non-Hermitian generalizations of the SSH model may be realized by cold-atom quantum simulators. Other quantum simulators, for example those use photonics [40], may also be suitable for demonstrating non-Hermitian behavior.

On the other hand, it has been demonstrated that one may use classical electric circuits to mimic the behavior of topological systems [41], and the circuit-analogue of the SSH model has been realized. It is also possible to introduce non-Hermitian effects by engineering the circuit simulators [42]. The non-Hermitian skin effect has been demonstrated recently [43]. Therefore, the non-Hermitian generalizations of the SSH model may also find their realizations in electric-circuit simulators. One advantage of using the cold-atom or circuit simulators to study the non-Hermitian effects discussed here is the broad tunability of the parameters in the simulators, which will allow a systematic verification of the phenomena without distractions from irrelevant material properties.

We mention that the dynamics of the Hermitian SSH

model can lead to quantized transport, which also has been demonstrated in cold-atom systems [44, 45]. Moreover, the topological edge states of the SSH model are proposed to cause quantum memory effects in boundary-induced dynamics [46]. Therefore, future research integrating quantum dynamics and non-Hermitian effects is expected to unveil more exciting dynamical phenomena.

V. CONCLUSION

By combining the generalizations of higher periods of the hopping coefficients and non-Hermitian effect, we have presented interesting physics of the non-Hermitian SSH3 and SSH4 models. While the Hermitian SSH3 model is topologically trivial, adding the non-Hermitian effect transforms it to a topological system with a point gap on the complex plane, characterized by the winding number. The non-Hermitian SSH3 model exhibits two types of localized states and one zero-energy state, but they are not associated with the topology. The SSH4 model is, in many aspects, the original SSH model in disguise. Nevertheless, the non-Hermitian SSH4 model exhibits the non-Hermitian skin effect, causing the skewed profiles of the bulk states. By considering the generalized Brillouin zone or the real-space winding number, the bulk-boundary correspondence of the non-Hermitian SSH4 model is restored. The phenomena presented here may be realized in cold-atom systems or other simulators, and the results will offer more examples of interesting non-Hermitian topological systems.

ACKNOWLEDGMENTS

Y. H was supported by the National Natural Science Foundation of China under Grant No. 11874272.

-
- [1] W. P. Su, J. R. Schrieffer, and A. J. Heeger, *Phys. Rev. Lett.* **42**, 1698 (1979).
 - [2] J. K. Asbóth, L. Oroszlány, and A. Pályi, *A Short Course on Topological Insulators: Band-structure topology and edge states in one and two dimensions* (Springer, Berlin, Germany, 2016).
 - [3] C.-K. Chiu, J. C. Y. Teo, A. P. Schnyder, and S. Ryu, *Rev. Mod. Phys.* **88**, 035005 (2016).
 - [4] M. Atala, M. Aidelsburger, J. T. Barreiro, D. Abanin, T. Kitagawa, E. Demler, and I. Bloch, *Nat. Phys.* **9**, 795 (2013).
 - [5] R. Drost, T. Ojanen, A. Harju, and P. Liljeroth, *Nat. Phys.* **13**, 668 (2017).
 - [6] S. D. Huber, *Nat. Phys.* **12**, 621 (2016).
 - [7] C. C. Chien, K. A. Velizhanin, Y. Dubi, B. R. Ilic, and M. Zwolak, *Phys. Rev. B* **97**, 125425 (2018).
 - [8] Y. He, K. Wright, S. Kouachi, and C. C. Chien, *Phys. Rev. A* **97**, 023618 (2018).
 - [9] M. Maffei, A. Dauphin, F. Cardano, M. Lewenstein, and P. Massignan, *New J. Phys.* **20**, 013023 (2018).
 - [10] D. Xie, W. Gou, T. Xiao, B. Gadway, and B. Yan, *npj Quantum Inf.* **5**, 55 (2019).
 - [11] C. M. Bender, *Rep. Prog. Phys.* **70**, 947 (2007).
 - [12] R. El-Ganainy, K. G. Makris, M. Khajavikhan, Z. H. Musslimani, S. Rotter, and D. N. Christodoulides, *Nat. Phys.* **14**, 11 (2018).
 - [13] Y. Ashida, Z. Gong, and M. Ueda, *Non-hermitian physics* (2020), arXiv:2006.01837.
 - [14] S. Yao and Z. Wang, *Phys. Rev. Lett.* **121**, 086803 (2018).
 - [15] S. Yao, F. Song, and Z. Wang, *Phys. Rev. Lett.* **121**, 136802 (2018).
 - [16] C. Yu, *Phys. Rev. A* **99**, 032109 (2019).
 - [17] K. Yokomizo and S. Murakami, *Phys. Rev. Lett.* **123**, 066404 (2019).
 - [18] F. K. Kunst, E. Edvardsson, J. C. Budich, and E. J. Bergholtz, *Phys. Rev. Lett.* **121**, 026808 (2018).

- [19] D. Leykam, K. Y. Bliokh, C. Huang, Y. D. Chong, and F. Nori, *Phys. Rev. Lett.* **118**, 040401 (2017).
- [20] K. I. Imura and Y. Takane (2019), arXiv: 1908.09438.
- [21] R. Koch and J. C. Budich, *Bulk-boundary correspondence in non-hermitian systems: Stability analysis for generalized boundary conditions* (2019), arXiv: 1912.07687.
- [22] F. Song, S. Yao, and Z. Wang, *Phys. Rev. Lett.* **123**, 170401 (2019).
- [23] Z. Li and R. S. K. Mong, *Homotopical classification of non-hermitian band structures* (2019), arXiv: 1911.02697.
- [24] C. C. Wojcik, X. Q. Sun, T. Bzdusek, and S. Fan, *Topological classification of non-hermitian hamiltonians* (2019), arXiv: 1911.12748.
- [25] W. X, Z. H. Zhang, Z. C. Gu, and W. Q. Chen, *Classification of topological phases in one dimensional interacting non-hermitian systems and emergent unitarity* (2019), arXiv: 1911.01590.
- [26] T. Bessho, K. Kawabata, and M. Sato, *Topological classification of non-hermitian gapless phases: Exceptional points and bulk fermi arcs* (2019), arXiv: 1911.08998.
- [27] H. Zhou and J. Y. Lee, *Phys. Rev. B* **99**, 235112 (2019).
- [28] A. Ghatak and T. Das, *J. Phys.: Condens. Matter* **31**, 263001 (2019).
- [29] L. Jin, *Phys. Rev. A* **96**, 032103 (2017).
- [30] Z. Gong, Y. Ashida, K. Kawabata, K. Takasan, S. Higashikawa, and M. Ueda, *Phys. Rev. X* **8**, 031079 (2018).
- [31] K. Kawabata, K. Shiozaki, M. Ueda, , and M. Sato, *Phys. Rev. X* **9**, 041015 (2019).
- [32] N. Hatano and D. R. Nelson, *Phys. Rev. Lett.* **77**, 570 (1996).
- [33] Y. Xiong, *J. Phys. Commun.* **2**, 035043 (2018).
- [34] G. W. Semenoff (2020), arXiv: 2003.11131.
- [35] F. Song, S. Yao, and Z. Wang, *Phys. Rev. Lett.* **123**, 246801 (2019).
- [36] A. Kitaev, *Annals of Physics* **321**, 2 (2006).
- [37] E. Prodan, T. L. Hughes, and B. A. Bernevig, *Phys. Rev. Lett.* **105**, 115501 (2010).
- [38] J. Zak, *Phys. Rev. Lett.* **62**, 2747 (1989), ISSN 00319007, 1508.02908.
- [39] W. Gou, T. Chen, D. Xie, T. Xiao, T. S. Deng, B. Gadway, W. Yi, and B. Yan, *Tunable non-reciprocal quantum transport through a dissipative aharonov-bohm ring in ultracold atoms* (2020), arXiv: 2001.01859.
- [40] X. Zhu, H. Wang, S. K. Gupta, H. Zhang, B. Xie, M. Lu, and Y. Chen, *Phys. Rev. Research* **2**, 013280 (2020).
- [41] C. H. Lee, S. Imhof, C. Berger, F. Bayer, J. Brehm, L. W. Molenkamp, T. Kiessling, and R. Thomale, *Comm. Phys.* **1**, 39 (2018).
- [42] T. Helbig, T. Hofmann, S. Imhof, M. Abdelghany, T. Kiessling, L. W. Molenkamp, C. H. Lee, A. Szameit, M. Greiter, and R. Thomale, *Observation of bulk boundary correspondence breakdown in topoelectrical circuits*, arXiv: 1907.11562.
- [43] T. Hofmann, T. Helbig, F. Schindler, N. Salgo, M. Brzezinska, M. Greiter, T. Kiessling, D. Wolf, A. Vollhardt, A. Kabasi, et al., *Phys. Rev. Research* **2**, 023265 (2020).
- [44] S. Nakajima, T. Tomita, S. Taie, T. Ichinose, H. Ozawa, L. Wang, M. Troyer, and Y. Takahashi, *Nat. Phys.* **12**, 296 (2016).
- [45] M. Lohse, C. Schweizer, O. Zilberberg, M. Aidelsburger, and I. Bloch, *Nat. Phys.* **12**, 350 (2016).
- [46] Y. He and C.-C. Chien, *Phys. Rev. B* **94**, 024308 (2016).